ARTICLE

Ultra-High Vacuum Scanning Thermal Microscopy for Nanometer Resolution Quantitative Thermometry

Kyeongtae Kim,[†] Wonho Jeong,[†] Woochul Lee,[†] and Pramod Reddy[‡,*,†]

[†]Department of Mechanical Engineering and [‡]Department of Materials Science and Engineering, University of Michigan, Ann Arbor, 48109

ABSTRACT

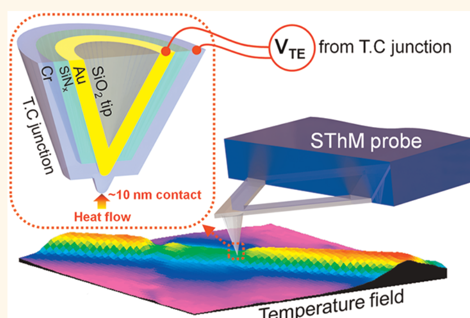

Understanding energy dissipation at the nanoscale requires the ability to probe temperature fields with nanometer resolution. Here, we describe an ultra-high vacuum (UHV)-based scanning thermal microscope (SThM) technique that is capable of quantitatively mapping temperature fields with ~15 mK temperature resolution and ~10 nm spatial resolution. In this technique, a custom fabricated atomic force microscope (AFM) cantilever, with a nanoscale Au–Cr thermocouple integrated into the tip of the probe, is used to measure temperature fields of surfaces. Operation in an UHV environment eliminates parasitic heat transport between the tip and the sample enabling quantitative measurement of temperature fields on metal and dielectric surfaces with nanoscale resolution. We demonstrate the capabilities of this technique by directly imaging thermal fields in the vicinity of a 200 nm wide, self-heated, Pt line. Our measurements are in excellent agreement with computational results—unambiguously demonstrating the quantitative capabilities of the technique. UHV-SThM techniques will play an important role in the study of energy dissipation in nanometer-sized electronic and photonic devices and the study of phonon and electron transport at the nanoscale.

KEYWORDS: scanning thermal microscopy · ultrahigh vacuum · quantitative temperature profiling · nanoscale thermal contact · thermocouple probe

Nanometer resolution thermometry is critical for probing and understanding energy dissipation in a variety of electronic and photonic devices.[1,2] It also plays an important role in fundamental studies of transport in nanoscale devices.[3−8] The wide applicability and importance of nanoscale thermometry has spurred the development of various experimental techniques that can be used to obtain information regarding temperature fields with nanometer to micrometer spatial resolution.[7−22] Among these techniques, scanning thermal microscopy (SThM), an atomic force microscope (AFM) based technique, has succeeded in achieving high spatial resolutions (~50 nm) on dielectric and metal surfaces.

Although impressive progress has been achieved in scanning thermal microscopy, obtaining quantitative information regarding thermal fields using SThM has remained elusive. Further, achieving high spatial resolutions of ~10 nm or lower has also not been possible despite the need for such resolution in detailed thermal studies on nanoscale devices. These apparent limitations of SThM arise due to operation in ambient conditions where local measurement of temperature fields is impeded by parasitic heat transfer between the tip and the sample *via* conduction through both air and the liquid meniscus that exists at the tip−sample interface. Further, the spatial resolution of SThM in the ambient is limited to ~50 nm due to the large tip−sample contact size (~50 nm) that arises from the liquid film existing at the tip−sample interface.[23] For example, Shi *et al.*[8] reported that the liquid meniscus imited temperature resolution of ambient SThM, in measurements of heat dissipation in carbon nanotubes, is ~50 nm. Recently, one of us in collaboration with others[17] reported a significant advance in the SThM technique where the effect of parasitic thermal transport through air was deconvoluted by performing additional scans and using a mathematical model. This improvement partially overcomes the challenge of obtaining quantitative measurement of thermal fields and enables thermometry with a temperature resolution of ~55 mK and a liquid meniscus limited spatial resolution of ~50 nm.

* Address correspondence to pramodr@umich.edu.

Received for review February 21, 2012 and accepted April 24, 2012.

Published online April 24, 2012
10.1021/nn300774n

© 2012 American Chemical Society

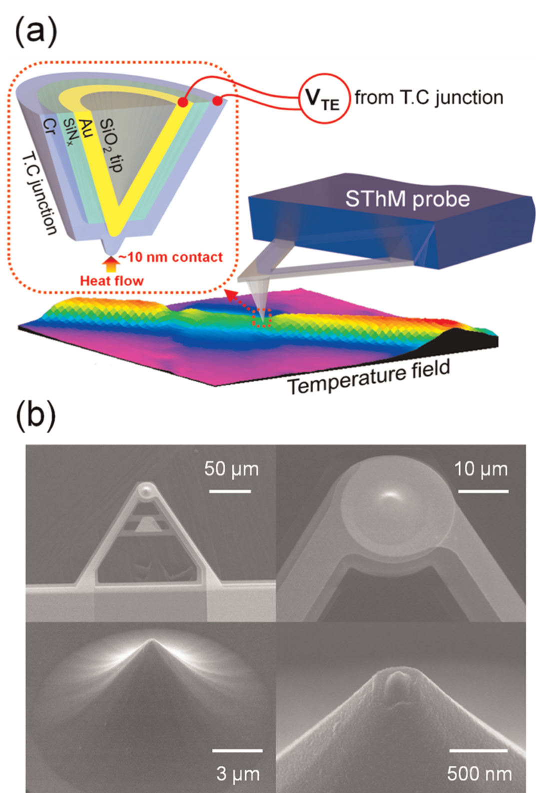

Figure 1. (a) Schematic illustrating the scanning thermal microscopy (SThM) technique described in this work. The Au–Cr nano thermocouple junction is at the end of the tip. Heat transfer between the tip and the sample is dominated by solid tip–sample contact whose diameter is ~10 nm. The thermoelectric voltage generated from the Au–Cr junction is directly proportional to the local temperature of the sample at the point contact and enables quantitative temperature measurements. (b) Scanning electron microscope images of the SThM probe with an integrated Au–Cr thermocouple. The Au–Cr thermocouple junction is at the end of the tip and the diameter of the tip end is ~100 nm.

In this paper, we overcome some of the major limitations of traditional SThM and unambiguously demonstrate the feasibility of performing quantitative nanoscale thermometry using UHV-SThM. Specifically, we demonstrate that it is possible to quantitatively measure temperature fields with excellent thermal (~15 mK) and spatial (~10 nm) resolutions. The improvement in spatial resolution is possible due to the absence of the liquid film at the tip–sample interface.[17] Further, quantitative local temperature measurements can be accomplished because heat transfer is dominated by the solid–solid contact (diameter of ~10 nm) between the probe and the sample. We note that recently Menges *et al.*[24] have also demonstrated a high vacuum scanning thermal imaging technique, that uses resistive thermal probes, to achieve quantitative thermal imaging with a spatial resolution[25] of ~25 nm and a temperature resolution of ~10 K. Although, UHV based techniques for thermal imaging of metallic surfaces[26] exist, we do not discuss them here as they are not applicable to dielectric surfaces. Next, we provide a detailed description of the

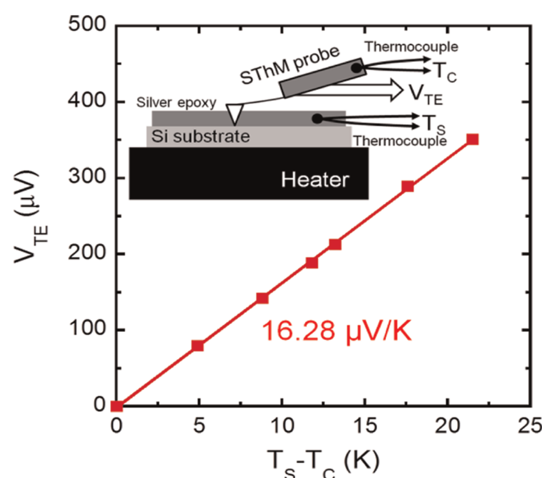

Figure 2. Measured thermoelectric voltage (V_{TE}) of the Au–Cr junction as a function of temperature difference ($T_S - T_C$) between the Au–Cr junction and the cantilevered probe body. The temperature of the tip (T_{tip}) and the sample (T_S) are assumed to be the same due to the excellent thermal contact between the tip and the sample. The inset shows the measurement setup used in the experiments.

UHV-SThM technique developed by us and describe its capabilities and limitations.

RESULTS AND DISCUSSION

A detailed schematic of the custom-fabricated SThM probe used in this study is shown in Figure 1 along with a scanning electron microscope (SEM) image of the fabricated probe. The SThM cantilever is ~0.5 μm thick and ~140 μm long and is created from low pressure chemical vapor deposition (LPCVD) silicon nitride (SiN_x). A groove is incorporated into the cantilever to achieve an effective stiffness constant of 4.0 ± 0.2 N/m (details in Supporting Information (SI)). The tip of the cantilever is created from low temperature silicon dioxide (LTO) and is approximately 8 μm tall. The gold (Au) and chrome (Cr) layers are ~100 nm thick and are isolated from each other at all regions except the tip end by ~70 nm of plasma-enhanced chemical vapor deposition (PECVD) SiN_x (Figure 1). The SEM pictures of the fabricated devices (Figure 1) show that the diameter of the tip of the fabricated SThM probe is ~100 nm and the Au–Cr thermocouple is ~200 nm in spatial extent and located at the very end of the tip. More details on the fabrication of SThM probes are provided in the Supporting Information.

Measurement of the Effective Seebeck Coefficient of the Au–Cr Junction. To characterize the effective Seebeck coefficient ($S_{junction}$) of the Au–Cr thermocouple integrated into the SThM probe, we pursued an approach similar to that adapted by others previously.[17,23] The SThM probe was mounted onto a substrate that has an electrical heater attached to it as shown in Figure 2 inset. Good thermal contact between the substrate and the tip was achieved by attaching the tip to the substrate *via* a thermally conducting epoxy. Further, two thermocouples were attached to the substrate and

the cantilever as shown in Figure 2. The temperature of the substrate was then increased in steps using the electrical heater, while temperatures of the substrate (T_S) and the cantilever (T_C) were recorded from the thermocouples attached to the substrate and the cantilever. The thermoelectric voltage across the Au−Cr junctions (V_{TE}) was also recorded as the temperature was increased and is reported in Figure 2. Given the excellent thermal contact between the tip and the substrate, the tip temperature (T_{tip}) can be assumed to be the same as the substrate temperature ($T_S = T_{tip}$). Therefore, the measured thermoelectric voltage (V_{TE}) can be directly related to the Seebeck coefficient of the junction by $V_{TE} = S_{junction} \times (T_S - T_C)$. From the data shown in Figure 2, the Seebeck coefficient ($S_{junction}$) of the Au−Cr junction is estimated to be 16.28 ± 0.15 μV/K. This measured Seebeck coefficient is in good agreement with that of similar probes fabricated in previous studies.[17,23]

Characterizing the Sensitivity of the SThM Probes in UHV. We define the sensitivity of the SThM probe as the rise in the temperature of the tip, as measured by the Au−Cr thermocouple, per unit temperature rise in the sample. In general, the temperature rise of the probe is not the same as that of the sample with which it is in contact. This difference in the tip and sample temperatures is due to the large thermal contact resistance between the tip and the sample. Further, it is to be expected that the sensitivity of the SThM probe would depend on various factors including the materials of the tip and the substrate, and the force applied on the cantilever which determines the contact diameter.

In past work by Shi *et al.*,[23] it was shown that the sensitivity of the SThM probe, operating in ambient conditions, depends on the size of the region that is being heated. Specifically, it was shown that when an SThM probe was placed in contact with a 5 μm wide platinum (Pt) line, which was heated electrically, the measured sensitivity was ∼0.5 K/K. Whereas, when the same tip was placed in contact with a heated 350 nm wide Pt line the sensitivity reduced dramatically to ∼0.05 K/K. This large variation in the sensitivity arises due to the parasitic heat conduction between the tip and the sample and makes it impossible to directly perform quantitative thermal measurements using SThM probes under ambient conditions.

To measure the sensitivity of SThM probe and unambiguously demonstrate the invariance of its sensitivity in an UHV environment we employed three different Pt lines that were all 50 nm thick and 200 nm, 1 μm, and 5 μm wide, respectively. All the Pt lines were deposited on a 600 nm thick SiO_2 layer that was thermally grown on a silicon wafer (more details in the SI). Further, an ∼10 nm thick layer of aluminum oxide (Al_2O_3) was conformally deposited using atomic layer deposition (ALD) on all the platinum lines. This thin layer of Al_2O_3 serves two important purposes: (1) it prevents accidental electrical shorts between the chrome layer of the tip and the Pt on the heater line even if the native chrome oxide on the Cr layer is abraded during the experiment; (2) it enables the creation of identical tip−sample contact conditions on the entire sample. We note that the Al_2O_3 layer deposited by ALD is very thin and amorphous,[27] and has a very small thermal conductivity[28−30] (∼1 W/(m·K)). Therefore, the Al_2O_3 layer does not cause any appreciable perturbation in the temperature fields on the surface of the sample (more details in the SI).

All the platinum lines used in the experiment were patterned in a four probe configuration as shown in Figure 3a. To heat the Pt lines, an alternating current at a known frequency (f = 5 Hz) and amplitude (I_o) was supplied through the Pt line (the specific choice of the oscillation frequency, f = 5 Hz, is discussed in detail later). Because of Joule heating, the temperature of the line oscillates at 2f, leading to an oscillation of the line resistance at 2f. The voltage across the line oscillating at 3f (see Figure 3a) is related to the temperature oscillation of the line by $\Delta T(2f) = 2(\mathrm{d}T/\mathrm{d}R)V_{3f}/I_0$, where ΔT is the amplitude of temperature oscillation at 2f, R is the resistance of the line, and V_{3f} is the amplitude of the voltage oscillation across the line at 3f (details of the measurement of temperature coefficient of resistance dT/dR are provided in the SI).

Before measuring the sensitivity of the SThM probes it is necessary to choose the contact force at which the sensitivity of the probe is characterized. This is important because the measured sensitivity depends on the applied contact force. To determine the appropriate contact force, the SThM probe which was initially separated from a Pt line whose temperature was modulated at 2f = 10 Hz was slowly displaced toward the Pt line. During this process, the deflection of the SThM probe was recorded using an optical scheme.[31] The measured deflection was used to estimate the force on the cantilever from the known spring constant of the cantilever. Further, the temperature oscillations of the SThM tip at 2f (10 Hz) were also simultaneously recorded using a lock in amplifier (SR 830) in a bandwidth 0.26 Hz. Data obtained in one such experiment are shown in Figure 3b where it is clear that the force on the SThM probe is negligible when the probe is away from the sample. When the probe is in close proximity to the sample it suddenly jumps into contact due to the van der Waals forces between the tip and the sample. As soon as mechanical contact is established, the temperature oscillations of the tip (at 2f = 10 Hz) become detectable. After initial contact, the amplitude of the measured temperature signal increases monotonically as the contact force is increased until the signal saturates. This behavior can be understood by noting that as the tip-sample contact force increases, the tip and sample deform elastically resulting in a gradual increase in the contact diameter. However, after transition to plastic deformation the contact diameter no longer increases significantly thus

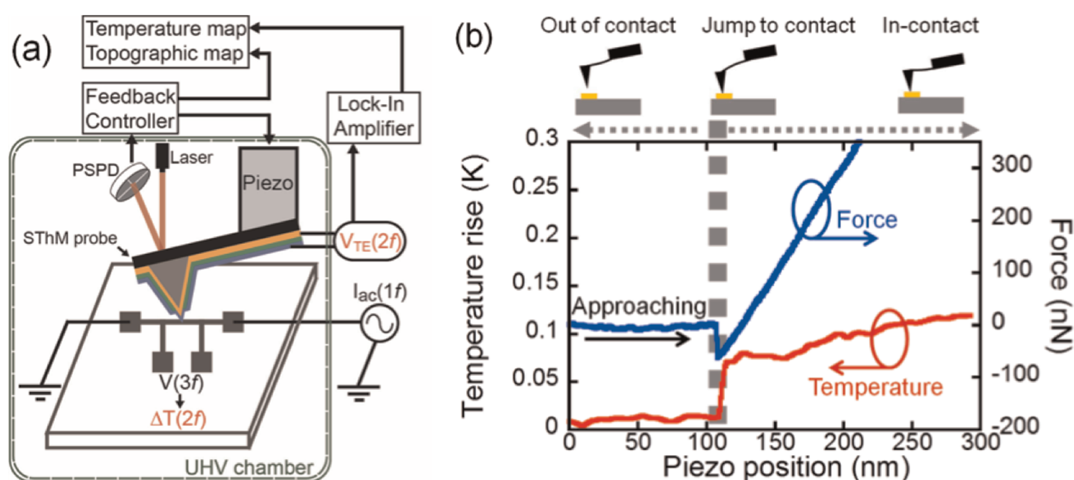

Figure 3. (a) A schematic of the experimental setup used in determining the sensitivity of the probe. The experiment is performed under UHV conditions (<10^{-9} Torr). A sinusoidal electrical current oscillating at *f* (5 Hz) is supplied through the platinum (Pt) line and causes temperature oscillations of the line at 2*f* (10 Hz). The temperature oscillation of the Pt line is measured by monitoring the oscillations in the resistance of the line. After the SThM pobe is placed in mechanical contact with the metal line the thermocouple voltage at 2*f* is recorded using a lock-in amplifier, and related to the local temperature using the measured effective Seebeck coefficient of the Au−Cr junction. (b) The measured force on the SThM probe and the measured temperature response of the probe are shown as a function of the piezo position in an experiment where the SThM probe was gradually displaced toward a 1 μm wide heated Pt line. A sudden jump in the temperature of the Au−Cr thermocouple is observed when the probe makes mechanical contact with the sample. The temperature of the thermocouple increases steadily when the tip is displaced further toward the sample due to an increase in the contact area between the tip and the sample.

resulting in saturation of the measured temperature oscillations. We note that it is clear from Figure 3b that a larger contact force results in a larger temperature sensitivity. However, a large contact force also increases the contact diameter, which results in a decrease in the spatial resolution. As a compromise, we apply a contact force of 150 ± 15 nN for all further characterizations as it corresponds to the smallest force where the measured thermal signal has almost saturated. The uncertainty of ±15 nN in the applied contact force arises from both the uncertainty in the spring constant of the cantilever and from the uncontrolled deflections of the cantilever due to bimaterial effects (details in the SI).

Given the contact force of 150 ± 15 nN, the contact diameter can be estimated using classical Hertzian theory:[1]

$$a_{\text{Hertz}} = \left(\frac{6rP}{E^*}\right)^{1/3} \quad (1)$$

where a_{Hertz} is the diameter of contact, r the tip radius (∼50 − 100 nm for SThM probes: see SI for details), P the applied load (150 nN), and $E^* = [(1 - \upsilon_1^2)/E_1 + (1 - \upsilon_2^2)/E_2]^{-1}$, the effective elastic modulus obtained from Young's moduli E_1 and E_2 and Poisson's ratios υ_1 and υ_2 of the tip and substrate surface materials. From eq 1, the contact diameter for a chromium-coated tip in contact with an Al_2O_3 surface is estimated to be ∼7 nm. Further, assuming elastic deformation the resulting pressure at the point contact can be estimated to be ∼6.8 GPa. However, if plastic deformation occurs, the contact diameter can be larger and can be estimated using[1]

$$a_{\text{plastic}} = \left(\frac{4P}{\pi H}\right)^{1/2} \quad (2)$$

where H is the hardness of the softer material (Cr) and is at least 1.0 GPa.[33,34] From this, the diameter for the applied contact force (150 nN) is estimated to be ∼13 nm. This discussion suggests that the tip-contact diameter is ∼10 nm for the applied contact force of 150 ± 15 nN. We note that one potential concern of imaging at such large forces is the possible damage to the tip due to shear forces. We investigated this effect in detail, and found that the deterioration was negligible even after continuous imaging for hours (details in the SI).

The sensitivity of the SThM probe was determined by performing experiments using three Pt lines which were 50 nm thick and 200 nm, 1 μm, and 5 μm wide, respectively. In each of the experiments, the amplitude of temperature oscillations of the tip (at 2*f* = 10 Hz) was recorded as a function of the amplitude of the temperature oscillations of the Pt line. The data obtained in each of these experiments is shown in Figure 4b from which the sensitivity of the SThM probe is estimated to be 0.034 ± 0.006 K/K and is independent of the line-width. This invariance of sensitivity with line-width is in strong contrast to past SThM work performed under ambient conditions where large variations in sensitivity were observed[23] when the line-width was changed. This invariance can be easily understood by noting that heat transport from the Pt line to the tip is primarily dominated by the ∼10 nm diameter tip−sample

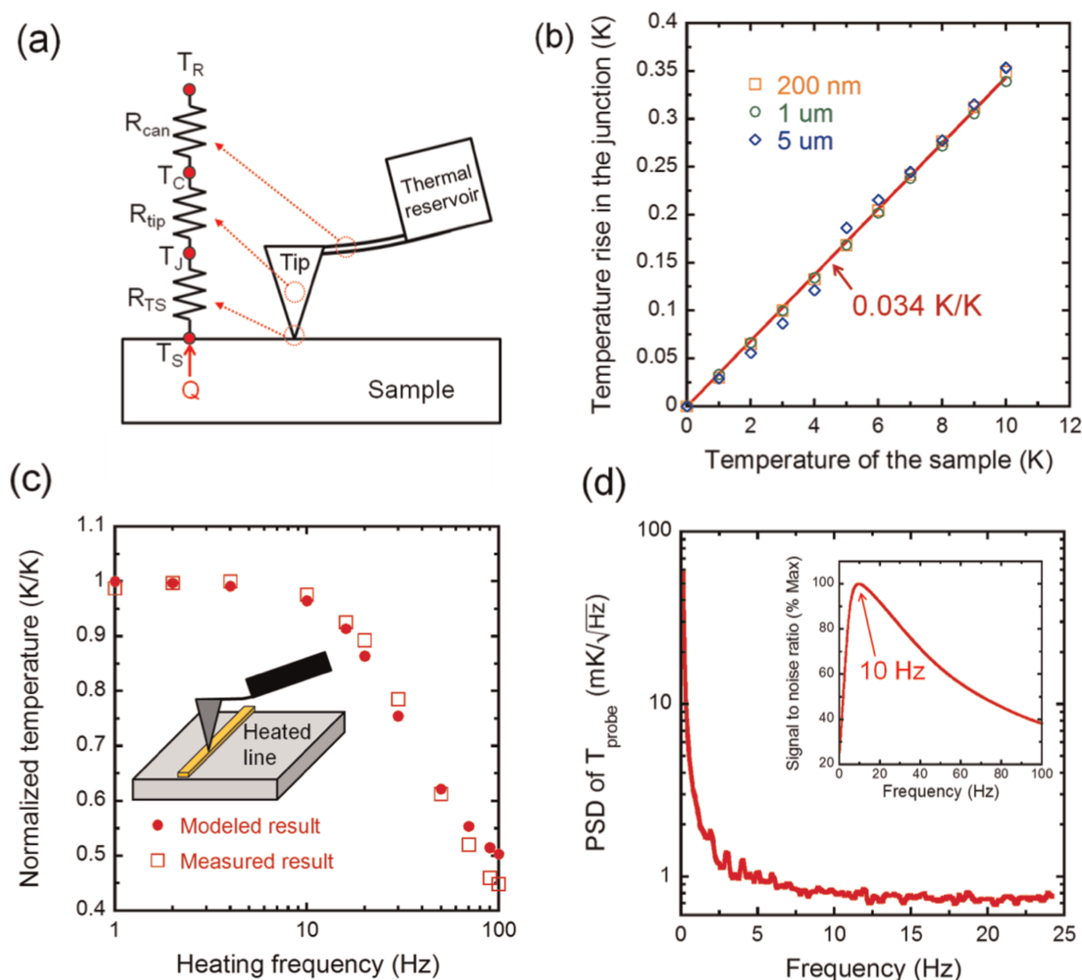

Figure 4. (a) A resistance network to model the thermal resistances at the tip−sample contact and the cantilever. (b) The measured temperature rise of the Au−Cr thermocouple junction as a function of temperature rise in the 5 μm, 1 μm, and 200 nm wide lines. The tip is in mechanical contact with Pt line with a contact force of ~150 nN. (c) The measured and modeled frequency responses of the SThM probe when the probe is in contact with a heated Pt line with a contact force of ~150 nN. (d) The measured power spectral density of thermal noise in the Au−Cr thermocouple junction of the SThM probe. The inset shows the signal-to-noise ratio (S/N) at different frequencies.

contact while all other mechanisms for heat transfer between the tip and the sample such as conduction through air molecules and near field radiation are negligible.

The measured sensitivity of the UHV-SThM probe is smaller than what was observed in the past for similar probes operating in ambient conditions. The reduced sensitivity is primarily due to the larger tip−sample contact thermal resistance that exists in UHV conditions as parasitic heat transport pathways between the tip and the sample are eliminated. A simple resistance network picture provided in the inset of Figure 4a can be used to estimate the expected sensitivity for a UHV-SThM probe. From the resistance network the sensitivity can be expressed as

$$\text{sensitivity} = \frac{R_C}{R_C + R_{TS}} \quad (3)$$

where $R_C = R_{tip} + R_{can}$ is the sum of the thermal resistances of the cantilever (R_{can}) and the tip (R_{tip}), whereas R_{TS} is the thermal resistance of the contact between the tip and the sample. The thermal resistance of the cantilever and the tip can be estimated from a knowledge of the geometry of the SThM probe and thermal conductivities of the various materials from which the probe is made and is found to be ~5×10^6 K/W (SI). The thermal contact resistance (R_{SS}) at a solid−solid point contact between a conical shaped object and a semi-infinite solid can be approximately obtained using the following expression:[1]

$$R_{ss} = \left[\pi a \left(\frac{k_{sm} k_{tip} \tan\theta}{2k_{sm} + k_{tip} \tan\theta}\right)\right]^{-1} \quad (4)$$

where k_{tip} and k_{sm} are the thermal conductivities of the conical tip and semi-infinite solid respectively, a is the diameter of the point contact (~10 nm) and θ (~21°) is the half angle of the conical tip. The tip−sample contact resistance can be obtained approximately using the above formula by approximating the sample

as a semi-infinite solid with a thermal conductivity k_{sm} of ~1 W/(m·K) as it comprises a thin film of amorphous Al_2O_3 and ~600 nm of SiO_2. Further, we approximate the tip to be equivalent to one made completely of SiO_2, therefore, k_{tip} is ~1 W/(m·K). Under these assumptions, the thermal resistance of the tip–sample contact (R_{TS}) can be estimated to be $\sim 2 \times 10^8$ K/W. This estimate is in good agreement with a more detailed model (see SI) that predicts a contact resistance of $\sim 10^8$ K/W. Further, the estimated resistance is in good agreement with past estimates of thermal resistance by Shi *et al.*[23] ($\sim 1.5 \times 10^8$ K/W) and Luo *et al.*[20] ($\sim 4 \times 10^8$ K/W). Using eq 3, and the estimated thermal resistances, the sensitivity can be estimated to be ~0.02 K/K. This value is in reasonable agreement with the measured sensitivity.

Thermal Time Constant. The frequency of operation ($2f$ = 10 Hz) was determined by measuring the thermal time constant of the SThM probe and noise spectral density of the Au–Cr thermocouple. The thermal time constant of the SThM probe was obtained by measuring the temperature rise of the tip at various heating frequencies while the amplitude of the heating current was held constant. A normalized temperature response obtained in such an experiment is shown in Figure 4c. The measured temperature response is found to be constant until ~10 Hz and decreases monotonically afterward. The thermal time constant (τ_{th}) of the tip is defined as $\tau_{th} = (2\pi f_R)^{-1}$, where f_R is the roll-off frequency which is defined as the frequency at which the normalized temperature is $1/\sqrt{2}$ K/K. Because the roll-off frequency is ~40 Hz (Figure 4c), the thermal time constant of the probe (τ_{th}) is ~4 ms. To confirm that the measured frequency response is consistent with the device geometry and the estimated tip–sample contact resistance, we analyzed the experimental results using a time-dependent finite difference model (see SI). The modeled result is shown along with the experimentally measured frequency response in Figure 4c and is seen to agree well with the experimentally obtained frequency response.

To obtain the signal-to-noise (S/N) ratio, we measured the noise in thermoelectric (V_N) voltage of the Au–Cr junction in a configuration where the tip is in contact with an unheated Pt line. The measured thermoelectric noise voltage is converted into an equivalent temperature noise (ΔT_N) using the known effective Seebeck coefficient of the Au–Cr junction ($\Delta T_N = V/S_{junction}$). The power spectral density (PSD) of the temperature noise signal is reported in Figure 4d and shows that the measured noise increases with decreasing frequencies. The signal-to-noise (S/N) ratio at various frequencies was obtained by first fitting polynomial curves to the signal and PSD curves and subsequently dividing the signal (Figure 4c) with the noise obtained from the PSD in a bandwidth of ~0.26 Hz (the same bandwidth used in obtaining the signal shown in Figure 4c). The obtained S/N ratio is shown in the inset of Figure 4d and features a peak in the S/N ratio at ~10 Hz suggesting that, for the probes used in this work, the optimal temperature modulation frequency for thermal imaging is ~10 Hz.

Demonstration of Quantitative Temperature Measurement. A predetermined sinusoidal electrical current was supplied through a 1 μm wide Pt line, fabricated on top of a 600 nm thick SiO_2 film which was located on a Si substrate, to create sinusoidal temperature oscillations at 10 Hz with an amplitude of 3 K. To demonstrate the quantitative measurement capabilities of UHV-SThM we directly measured the temperature profile of the surface in a direction perpendicular to the Pt line by performing a line-scan as shown in Figure 5a and compared it with a profile obtained from Finite Element Modeling (modeling details in SI). Figure 5b shows the topographical profile of the Pt line along with the measured and modeled temperature profiles which are in excellent agreement with each other suggesting that UHV-SThM can quantitatively measure temperature fields. This result is particularly significant because it is in strong contrast to SThM performed under ambient conditions[23] where large deviations between the measured and modeled temperature profiles were observed.

In addition to measuring the temperature profile of the 1 μm wide Pt line, we also studied the temperature profile of a 200 nm wide line whose temperature was oscillating at 10 Hz with an amplitude of 6 K. Specifically, we performed line-scans perpendicular to the 200 nm line at two different scan rates: one scan was performed slowly (at a speed of ~50 nm/second), whereas the second scan was performed at a faster rate (at a speed of ~200 nm/second) which was comparable to the scan rate of the 1 μm wide Pt line discussed earlier. The temperature profiles obtained in the slow and fast scans are shown in Figure 5 panels c and d, respectively, along with the topographical profile of the Pt line and the modeled temperature profiles. The measured data shown in Figure 5d (fast scan) are found to be in excellent agreement with the computed profile. However, the data obtained in the slow scan show features that deviate significantly from the computed temperature profiles near the line edge. This deviation from the modeled temperature profile can be understood by noting that sudden changes in contact area between the tip and the sample occurs when the tip moves spatially from the top of the Pt line located near the edge of the Pt line to a neighboring point on the sample or vice versa (see Figure 5c inset). This change in the contact area results in a corresponding change in the thermal resistance between the tip and the sample resulting in a spurious measurement. However, these features are not visible in a fast scan due to spatial averaging of data that occurs because of the fast scan rate. We note that such edge effects have

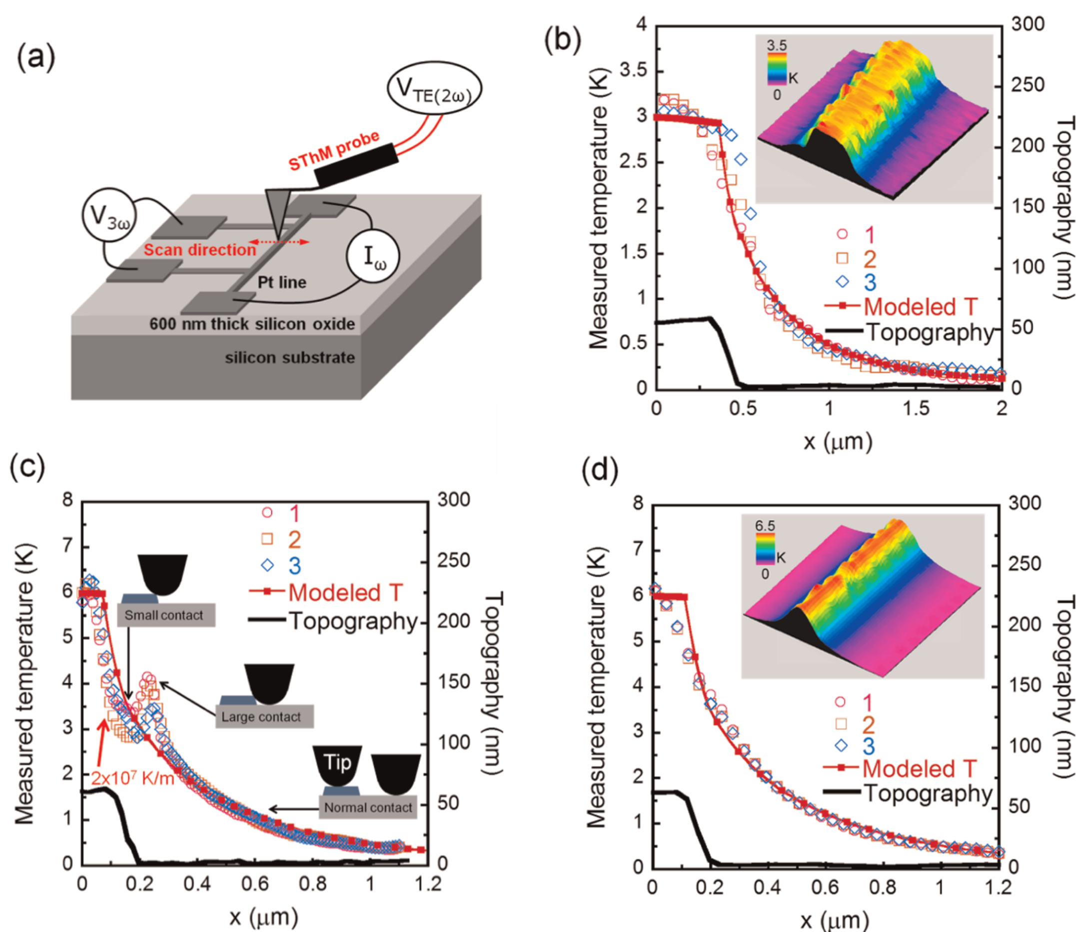

Figure 5. (a) A schematic diagram of the setup used to demonstrate quantitative thermal measurements. The temperature and topography around a heated Pt line are simultaneously obtained by scanning in a direction perpendicular to the Pt line. (b) The topographical profile of the Pt line along with the measured and modeled temperature profiles are shown. The inset of the figure depicts a three-dimensional map of the temperature field measured on a section of the 1 μm wide Pt line. (c and d) The temperature profiles obtained in the slow and fast scans are shown in Figures c and d, respectively, along with the modeled temperature profiles and the topographical profile of the Pt line. The inset of Figure 5c depicts the contact conditions between the probe and the Pt line while scanning. Whereas, the inset of Figure 5d depicts a three-dimensional map of the temperature field measured on a section of the 200 nm wide Pt line.

also been observed in past SThM work in the ambient.[23,35] The results shown in Figure 5 unambiguously show that UHV-SThM is capable of performing quantitative thermal imaging; however, deviations from the true temperature can occur when there are steps in the topography. We believe that even this limitation could potentially be overcome by deconvoluting the edge effects from a knowledge of the topography of the sample, this is the focus of our future work.

Demonstration of Thermal Imaging. Since the thermocouple is integrated into the tip of the SThM probe it is possible to easily obtain both the topographical and thermal images. To demonstrate these capabilities we imaged a 2-dimensional temperature field. Specifically, we thermally imaged a region where the 200 nm wide Pt line (through which an electrical current is flowing) is connected to a 1 μm wide Pt line (probe lead through which no electrical current is passing, see Figure 6a). Figure 6b shows the topography of the region of interest, whereas Figure 6c shows the measured thermal field. As can be seen from the figure, the temperature rise of the 200 nm line is lower in the region where it intersects the 1 μm wide line because the 1 μm wide Pt line acts as a fin. In addition to this we also imaged the thermal fields in sections of the 200 nm and 1 μm wide lines (inset of Figure 5b,d). The obtained thermal images show a one-dimensional temperature field where the amplitude of temperature oscillations decays rapidly away from the line (detailed topographical and temperature images are provide in the SI).

Temperature Resolution of UHV-SThM. The temperature resolution of the UHV-SThM probes can be estimated from a knowledge of the PSD of the voltage noise (Figure 4d), and the measured sensitivity of the thermocouple (0.034 K/K). From the measured PSD the noise at the measurement frequency ($2f$ = 10 Hz) was found to be ~1 mK/(Hz)$^{1/2}$ (Figure 4d). This implies that in the measurement bandwidth (0.26 Hz) the root-mean-square noise voltage (ΔT_{noise}) is ~0.5 mK. The noise limited temperature resolution can be estimated

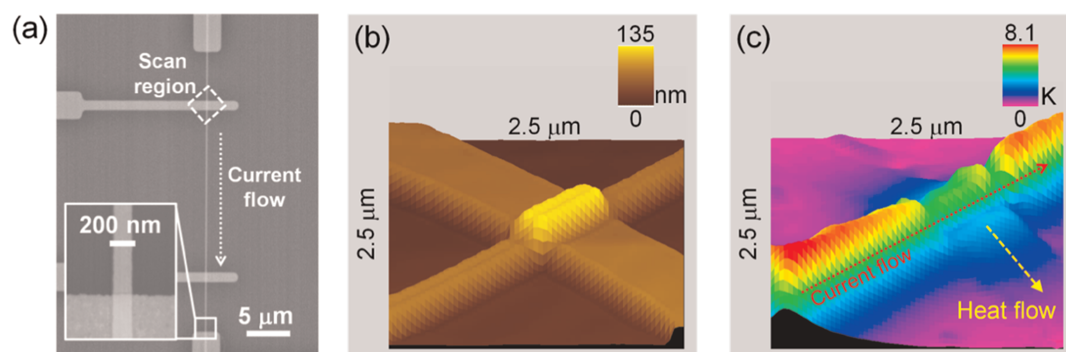

Figure 6. (a) Scanning electron microscope image of a 200 nm wide Pt line; (b) 3D topographic of a 2.5 μm × 2.5 μm region where the 200 nm wide Pt line lies on top of a 1 μm wide Pt line; (c) thermal image of the same region shown in panel b. The temperature rise of the 200 nm line is seen to be lower in the region where it intersects the 1 μm wide line because the 1 μm wide Pt line acts as a fin.

to be ($\Delta T_{resolution} = \Delta T_{noise}$/sensitivity) ~15 mK. The sensitivity of the measurement could be improved further by choosing a smaller bandwidth. However, such a reduction greatly increases the scanning time making it infeasible to dramatically reduce the bandwidth.

Spatial Resolution of UHV-SThM. The spatial resolution of thermal imaging techniques is related to the largest temperature gradient $|\vec{\nabla} T|_{max}$ that can be measured. Specifically, the spatial resolution (Δr) is usually defined as ($\Delta r = \Delta T_{resolution}/|\vec{\nabla} T|_{max}$). It can be seen from Figure 5c that temperature gradients as large as 2×10^7 K/m can be measured while scanning the probe from the center to the edge of the heated 200 nm wide Pt line. From this measured thermal gradient, the spatial resolution of the technique can be estimated to be ~1 nm. However, this estimate needs to be interpreted with caution because the contact diameter of the point contact is ~10 nm, resulting in a reduction of resolution due to spatial averaging. Therefore, we estimate the real spatial resolution of UHV-SThM to be ~10 nm—this represents the highest spatial resolution among all the nanoscale thermal imaging techniques reported until now.

We also note that the claimed spatial resolution is supported by the data in Figure 5c, where the measured and computed temperature profiles are shown in the vicinity of a 200 nm wide line. The computed and measured temperature profiles agree well with each other everywhere except at the line edge where the edge contact effects result in artifacts. In the region where we have excellent agreement, the data shows that the temperature difference between two neighboring points separated by ~10 nm is ~50 mK (see SI, Figure S13 for a detailed plot), and is easily detected by the probe that has a temperature resolution of ~15 mK. This unambiguously shows that the resolution of our probe is ~10 nm.

Limitations of the Technique. The UHV-SThM technique described in this work suffers from edge effects that complicate the measurement of temperature fields in regions where there is a sudden change in the topography of the sample: for example, the edge of a line (Figure 5c). This could potentially make it difficult to use this technique on rough surfaces. Further, due to variations in the tip geometry from probe to probe, it is necessary to perform the thermal signal *versus* applied force calibration shown in Figure 3b for each probe to determine the appropriate contact force at which to perform the scanning. This could be time-consuming and represents a limitation of the technique.

CONCLUSION

To summarize, we have demonstrated a scanning thermal microscopy technique capable of a spatial resolution of ~10 nm and a temperature resolution of ~15 mK. This high resolution is obtained by using a customized AFM probe, with an integrated nanoscale thermocouple, in an ultra-high vacuum environment. We demonstrated the quantitative capabilities of this technique by directly imaging thermal fields in the vicinity of a 200 nm wide, self-heated Pt line. Our measurements are found to be in excellent agreement with computational results—unambiguously demonstrating the quantitative capabilities of the technique. UHV-SThM is well suited for the study of nanoscale thermal transport and will play an important role in understanding energy dissipation, phonon transport, and electron–phonon interactions in nanoscale electronic and photonic devices.

METHODS

Finite Difference Modeling. To analyze the time constant of the probe and the tip–sample thermal contact resistance, it was necessary to compute the temperature fields in the SThM probe. To accomplish this, we used one of MATLAB's solvers, bvp4c, which can solve boundary value problems for ordinary differential equations (more details in the SI).

Finite Element Modeling. To obtain the temperature profile around heated Pt lines, we used COMSOL (general heat transfer module). By taking advantage of the symmetry of the temperature profile, only half of the actual geometry was used in the calculation, enabling the use of a finer mesh. A different COMSOL module (solid, stress-stain, smsld) was used in the calculation of cantilever stiffness and force uncertainty resulting from the bimaterial effect (more details in the SI).

SThM Measurements. We performed the thermal imaging in an ultra-high vacuum atomic force microscope (UHV 7500 VT System, RHK Technology). The vacuum level was below 10^{-9} Torr during the experiment. A constant force ($\sim$150 nN) was maintained during scanning to obtain the topographic and thermal maps. While obtaining the topographic map using RHK SPM 100 controller, the temperature oscillations of the SThM tip were simultaneously recorded using a lock-in amplifier (SR 830).

Conflict of Interest: The authors declare no competing financial interest.

Acknowledgment. Research supported by the U.S. Department of Energy, Office of Basic Energy Sciences, Division of Materials Sciences and Engineering under Award DE-SC0004871 (P.R., K.K.) and by an AFOSR grant from the Thermal Sciences Division FA9550-10-1-0528 (W.J.)

Supporting Information Available: Experimental details regarding the fabrication of the SThM probes and characterization of their stiffness and tip radius; details regarding fabrication of the Pt lines; the characterization of the temperature coefficient of resistance of the lines; finite element modeling of both the temperature fields and the effect of the aluminum oxide layer on the temperature fields; discussion of the measurement of the Seebeck coefficient of the Cr–Au junctions integrated into the probes; modeling performed to estimate the tip–sample contact thermal conductance; frequency response of the SThM probe; discussions of the effect of bimaterial effects on the contact force and the robustness of the SThM probes. This material is available free of charge *via* the Internet at http://pubs.acs.org.

REFERENCES AND NOTES

1. Majumdar, A. Scanning Thermal Microscopy. *Annu. Rev. Mater. Sci.* **1999**, *29*, 505–585.
2. Luo, K.; Herrick, R. W.; Majumdar, A.; Petroff, P. Scanning Thermal Microscopy of a Vertical-Cavity Surface-Emitting Laser. *Appl. Phys. Lett.* **1997**, *71*, 1604–1606.
3. Grosse, K. L.; Bae, M. H.; Lian, F. F.; Pop, E.; King, W. P. Nanoscale Joule Heating, Peltier Cooling and Current Crowding at Graphene–Metal Contacts. *Nat. Nanotechnol.* **2011**, *6*, 287–290.
4. Jo, I.; Hsu, I. K.; Lee, Y. J.; Sadeghi, M. M.; Kim, S.; Cronin, S.; Tutuc, E.; Banerjee, S. K.; Yao, Z.; Shi, L. Low-Frequency Acoustic Phonon Temperature Distribution in Electrically Biased Graphene. *Nano Lett.* **2010**, *11*, 85–90.
5. Kim, P.; Shi, L.; Majumdar, A.; McEuen, P. L. Mesoscopic Thermal Transport and Energy Dissipation in Carbon Nanotubes. *Phys. B: Condens. Matter* **2002**, *323*, 67–70.
6. Shi, L.; Plyasunov, S.; Bachtold, A.; McEuen, P. L.; Majumdar, A. Scanning Thermal Microscopy of Carbon Nanotubes Using Batch-Fabricated Probes. *Appl. Phys. Lett.* **2000**, *77*, 4295–4297.
7. Weaver, J. M. R.; Walpita, L. M.; Wickramasinghe, H. K. Optical-Absorption Microscopy and Spectroscopy with Nanometer Resolution. *Nature* **1989**, *342*, 783–785.
8. Shi, L.; Zhou, J. H.; Kim, P.; Bachtold, A.; Majumdar, A.; McEuen, P. L. Thermal Probing of Energy Dissipation in Current-Carrying Carbon Nanotubes. *J. Appl. Phys.* **2009**, *105*, 3126708–3126712.
9. Boroumand, F. A.; Voigt, M.; Lidzey, D. G.; Hammiche, A.; Hill, G. Imaging Joule Heating in a Conjugated-Polymer Light-Emitting Diode Using a Scanning Thermal Microscope. *Appl. Phys. Lett.* **2004**, *84*, 4890–4892.
10. Choi, S. H.; Lee, T. I.; Baik, H. K.; Roh, H. H.; Kwon, O.; Suh, D. h. The Effect of Electrode Heat Sink in Organic-Electronic Devices. *Appl. Phys. Lett.* **2008**, *93*, 183301.
11. Christofferson, J.; Shakouri, A. Thermoreflectance Based Thermal Microscope. *Rev. Sci. Instrum.* **2005**, *76*, 024903.
12. Fiege, G. B. M.; Feige, V.; Phang, J. C. H.; Maywald, M.; Gorlich, S.; Balk, L. J. Failure Analysis of Integrated Devices by Scanning Thermal Microscopy (SThM). *Microelectron. Reliab.* **1998**, *38*, 957–961.
13. Fiege, G. B. M.; Niedernostheide, F. J.; Schulze, H. J.; Barthelmeß, R.; Balk, L. J. Thermal Characterization of Power Devices by Scanning Thermal Microscopy Techniques. *Microelectron. Reliab.* **1999**, *39*, 1149–1152.
14. Fletcher, D. Thermal Microscopy with a Microfabricated Solid Immersion Lens. *Microscale Thermophys. Eng.* **2003**, *7*, 267–273.
15. Hammiche, A.; Bozec, L.; Conroy, M.; Pollock, H. M.; Mills, G.; Weaver, J. M. R.; Price, D. M.; Reading, M.; Hourston, D. J.; Song, M. Highly Localized Thermal, Mechanical, and Spectroscopic Characterization of Polymers Using Miniaturized Thermal Probes. *J. Vac. Sci. Technol., B* **2000**, *18*, 1322–1332.
16. Hammiche, A.; Hourston, D. J.; Pollock, H. M.; Reading, M.; Song, M. Scanning Thermal Microscopy: Subsurface Imaging, Thermal Mapping of Polymer Blends, and Localized Calorimetry. *J. Vac. Sci. Technol., B* **1996**, *14*, 1486–1491.
17. Kim, K.; Chung, J.; Hwang, G.; Kwon, O.; Lee, J. S. Quantitative Measurement with Scanning Thermal Microscope by Preventing the Distortion Due to the Heat Transfer through the Air. *ACS Nano* **2011**, *5*, 8700–8709.
18. Kwon, O. Cross-Sectional Thermal Imaging of a Metal-Oxide Semiconductor Field-Effect Transistor. *Microscale Thermophys. Eng.* **2003**, *7*, 349–354.
19. Lai, J.; Chandrachood, M.; Majumda, A.; Carrejo, J. P. Thermal Detection of Device Failure by Atomic Force Microscopy. *Electr. Dev. Lett., IEEE* **1995**, *16*, 312–315.
20. Luo, K.; Shi, Z.; Varesi, J.; Majumdar, A. Sensor Nanofabrication, Performance, and Conduction Mechanisms in Scanning Thermal Microscopy. *J. Vac. Sci. Technol., B* **1997**, *15*, 349–360.
21. Sadat, S.; Tan, A.; Chua, Y. J.; Reddy, P. Nanoscale Thermometry Using Point Contact Thermocouples. *Nano Lett.* **2011**, *10*, 2613–2617.
22. Nelson, B. A.; King, W. P. Measuring Material Softening with Nanoscale Spatial Resolution Using Heated Silicon Probes. *Rev. Sci. Instrum.* **2007**, *78*, 023702–9.
23. Shi, L.; Majumdar, A. Thermal Transport Mechanisms at Nanoscale Point Contacts. *J. Heat Transfer, Trans. ASME* **2002**, *124*, 329–337.
24. Menges, F.; Riel, H.; Stemmer, A.; Gotsmann, B. Quantitative Thermometry of Nanoscale Hot Spots. *Nano Lett.* **2012**, *12*, 596–601.
25. Hinz, M.; Marti, O.; Gotsmann, B.; Lantz, M. A.; Durig, U. High Resolution Vacuum Scanning Thermal Microscopy of HfO_2 and SiO_2. *Appl. Phys. Lett.* **2008**, *92*, 043122–3.
26. Muller-Hirsch, W.; Kraft, A.; Hirsch, M. T.; Parisi, J.; Kittel, A. Heat Transfer in Ultrahigh Vacuum Scanning Thermal Microscopy. *J. Vac. Sci. Technol., A* **1999**, *17*, 1205–1210.
27. Groner, M. D.; Fabreguette, F. H.; Elam, J. W.; George, S. M. Low-Temperature Al_2O_3 Atomic Layer Deposition. *Chem. Mater.* **2004**, *16*, 639–645.
28. Bai, S. Y.; Tang, Z. A.; Huang, Z. X.; Yu, J.; Wang, J. Q. Thermal Conductivity Measurement of Submicron-Thick Aluminium Oxide Thin Films by a Transient Thermo-Reflectance Technique. *Chin. Phys. Lett.* **2008**, *25*, 593–596.
29. Kato, R.; Maesono, A.; Tye, R. P. Thermal Conductivity Measurement of Submicron-Thick Films Deposited on Substrates by Modified AC Calorimetry (Laser-Heating Ångstrom Method). *Int. J. Thermophys.* **2001**, *22*, 617–629.
30. Lee, S. M.; Cahill, D. G.; Allen, T. H. Thermal-Conductivity of Sputtered Oxide-Films. *Phys. Rev. B* **1995**, *52*, 253–257.
31. Meyer, G.; Amer, N. M. Novel Optical Approach to Atomic Force Microscopy. *Appl. Phys. Lett.* **1988**, *53*, 1045–1047.
32. Bietsch, A.; Schneider, M. A.; Welland, M. E.; Michel, B. Electrical Testing of Gold Nanostructures by Conducting Atomic Force Microscopy. *J. Vac. Sci. Technol., B* **2000**, *18*, 1160–1170.

33. Samsonov, G. V. *Handbook of the Physicochemical Properties of the Elements*; IFI/Plenum: New York, 1968; p xii.
34. Kataria, S.; Goyal, S.; Dash, S.; Tyagi, A. K. Nanomechanical Characterization of Thermally Evaporated Cr Thin Films—FE Analysis of the Substrate Effect. *Thin Solid Films* **2010**, *519*, 312–318.
35. Kim, K.; Chung, J.; Won, J.; Kwon, O.; Lee, J. S.; Park, S. H.; Choi, Y. K. Quantitative Scanning Thermal Microscopy Using Double Scan Technique. *Appl. Phys. Lett.* **2008**, *93*, 203115–7.